**Lichen-Like Symbiosis 600 Million Years Ago**
Xunlai Yuan, *et al.*
*Science* **308**, 1017 (2005);
DOI: 10.1126/science.1111347

ing huge volcanic hydrogen outgassing rates or assuming a reduced mantle. The efficient production of organics in a hydrogen-rich early Earth's atmosphere would have led to an organic soup in the oceans and ponds on the early Earth. The world ocean could have been the birthplace of life (*14*).

### References and Notes


1. C. F. Chyba, C. Sagan, in *Comets and the Origin and Evolution of Life* (Springer, New York, 1997), pp. 147–173.
2. S. L. Miller, *Science* **117**, 528 (1953).
3. J. P. Pinto, G. R. Gladstone, Y. L. Yung, *Science* **210**, 183 (1980).
4. P. H. Abelson, *Proc. Natl. Acad. Sci. U.S.A.* **55**, 1365 (1966).
5. K. J. Zahnle, *J. Geophys. Res.* **91**, 2819 (1986).
6. V. M. Canuto, J. S. Levine, T. R. Augustsson, C. L. Imhoff, M. S. Giampapa, *Nature* **305**, 281 (1983).
7. G. Schlesinger, S. L. Miller, *J. Mol. Evol.* **19**, 376 (1983).
8. R. Stribling, S. L. Miller, *Orig. Life* **17**, 261 (1987).
9. Both $CH_4$ and $NH_3$ in the atmosphere of early Earth would have been subject to rapid loss driven by solar UV radiation. It is unlikely that the volcanic outgassing rate of $CH_4$ or $NH_3$ could have been adequate to maintain high concentrations of these gases.
10. The hydrogen concentration is determined by the balance between the volcanic outgassing rate of hydrogen and the escape of hydrogen to space. The modern volcanic hydrogen outgassing rate is $\sim 1.8 \times 10^{10}$ hydrogen molecules $cm^{-2}$ $s^{-1}$ (*29*). Because of higher heat flow in the past, the overall outgassing rate of gases, and hydrogen in particular, might have been ~5 times greater on ancient Earth (*30*). In the present Earth's atmosphere, oxygen is dominant at the exobase level (defined as the boundary beyond which rapidly moving molecules may escape without collision). The current exospheric temperature is high (1000 to 2500 K) because of the efficient absorption of solar UV radiation by oxygen. If the exospheric temperature on the early Earth were as high as it is today, Jeans escape of hydrogen from the atmosphere would have been efficient, and the diffusion of hydrogen through the background gases to the homopause level would have been the limiting process. The rate of diffusion-limited escape can be expressed as $F(H_2) = 2.5 \times 10^{13} f_{total}$ molecules $cm^{-2}$ $s^{-1}$, with $f_{total}$ defined as the total mixing ratio of hydrogen (in all chemical forms) at the homopause (*31*). By balancing the diffusion-limited escape rate of hydrogen with the hydrogen outgassing rate, the hydrogen mixing ratio up to the homopause in early Earth's atmosphere should be of the order of $10^{-3}$ or below (*21*, *31*), unless the oxidation state of Earth's mantle was more reduced than its current oxidation state. But Earth's mantle has been suggested to be in a similar oxidation state to that of today for the past 3.96 billion years (*32*). The common consensus among planetary scientists for the past 30 years has been that early Earth's atmosphere had a low hydrogen concentration.
11. However, experiments to date generate only methane or formate in realistic hydrothermal-like systems (*33*). The exogenous flux of organic materials at about 4 billion years ago (Ga), primarily interplanetary dust particles (IDPs), may be less than 150 times the present value (*34*), although the interpretations of the Akilia rocks are debatable (*35*).
12. J. C. G. Walker, *Orig. Life* **16**, 117 (1985).
13. I. de Pater, J. J. Lissauer, in *Planetary Sciences* (Cambridge Univ. Press, Cambridge, 2001), pp 66–71.
14. Materials and methods are available as supporting material on *Science* Online.
15. H. Lammer *et al.*, *Icarus* **165**, 9 (2003).
16. D. M. Hunten, *Planet. Space Sci.* **30**, 773 (1982).
17. S. Kumar, D. M. Hunten, J. B. Pollack, *Icarus* **55**, 369 (1983).
18. Nonthermal escape from a hydrogen-rich early Earth has not been studied in detail. Although a similar upper limit of nonthermal hydrogen escape rate should apply to early Earth, it is important to note that nonthermal hydrogen escape processes may also be rather different for Earth than for Venus because of the presence of a strong magnetic field on Earth. Future work should include these processes in escape models to make more accurate estimates.
19. J. D. Dorren, E. F. Guinan, *Astrophys. J.* **428**, 805 (1994).
20. Assuming that the linear relation between escape flux and EUV still holds for even higher solar EUV input, the hydrogen escape flux would be about $7.5 \times 10^{12}$ $cm^{-2}$ $s^{-1}$ for a solar EUV level 100 times that of today if the homopause hydrogen density is kept at $\sim 5 \times 10^{12}$ $cm^{-3}$. This escape rate is still slower than the diffusion-limited escape rate ($>1 \times 10^{13}$ $cm^{-2}$ $s^{-1}$) for the same homopause hydrogen density. Hence, the diffusive flux does not become limiting except for extreme EUV input.
21. J. F. Kasting, *Science* **259**, 920 (1993).
22. $H_2$ is not a chemically reactive gas. So in the steady state, hydrogen has a virtually constant mixing ratio all the way from the surface to the homopause, as does $CO_2$ (*21*). Therefore, the homopause mixing ratio of hydrogen is representative of the whole homosphere.
23. The amino acid production rate is found to be ~0.4 nmol $cm^{-2}$ $year^{-1}$ (*8*) in electric discharge experiments when $H_2/CO_2 = 4$, equivalent to $2 \times 10^8$ kg/year assuming a mean molecular weight of 100. This estimate is based on an annual electric discharge rate $\sim 2 \times 10^{19}$ J/year, which is ~20 times the contemporary electric discharge rate, $\sim 1 \times 10^{18}$ J/year (*36*). If the electric discharge rate on early Earth is the same as that of today, the rate of amino acid production by electric discharge would be $1 \times 10^7$ kg/year when $H_2/CO_2 = 4$. Extrapolating the contemporary data back to early Earth faces large uncertainty. So here the conservative estimate ($1 \times 10^7$ kg/year) of the amino acid production rate by electric discharge is taken.
24. Assuming the ocean volume is $1.4 \times 10^{21}$ liters and that there is no loss of organics within the ocean, the amino acid concentration in the ocean can reach $7 \times 10^{-8}$ kg/liter (equivalent to $7 \times 10^{-7}$ mole/liter, assuming a mean molecular weight of 100) in 10 million years, which is the time scale for the entire ocean to circulate through submarine vents at 300°C, potentially destroying the organics (*25*).
25. E. Pierazzo, C. F. Chyba, *Meteorit. Planet. Sci.* **34**, 909 (1999).
26. C. M. Dobson, G. B. Ellison, A. F. Tuck, V. Vaida, *Proc. Natl. Acad. Sci. U.S.A.* **97**, 11864 (2000).
27. A. A. Pavlov, J. F. Kasting, J. L. Eigenbrode, K. H. Freeman, *Geology* **29**, 1003 (2001).
28. It is difficult to estimate accurately how much organic material was delivered to early Earth by comets because of the large uncertainty in the impact record (*37*). The delivery of organic compounds by IDPs is more definitive, although still debatable. For the present Earth, the mass flux of all IDPs with particle mass lower than $10^{-6}$ g is $10^7$ kg/year (*38*). It is suggested that the IDP flux at 4 Ga could be up to ~150 times that of today (*34*), although the interpretation of the geological record leading to this suggestion is debatable. Bearing that in mind, a reasonable estimate of the organic delivery rate by IDP at 4 Ga is in the order of $\sim 10^8$ kg/year, assuming 10% of the mass is organic (*1*). The formation rate of prebiotic organic compounds in hydrothermal vents is also in the order of $10^8$ kg/year (*39*). Therefore, the production of prebiotic organic compounds by UV in a hydrogen-rich atmosphere is ~2 orders of magnitude greater than the delivery of organic compound from outer space or the synthesis of organic compounds in hydrothermal systems at 3.8 Ga.
29. H. D. Holland, *Geochim. Cosmochim. Acta* **66**, 3811 (2002).
30. D. L. Turcotte, *Earth Planet. Sci. Lett.* **48**, 53 (1980).
31. J. C. G. Walker, *Evolution of the Atmosphere* (Macmillan, New York, 1977).
32. J. W. Delano, *Orig. Life Evol. Biosph.* **31**, 311 (2001).
33. T. M. McCollom, J. S. Seewald, *Geochim. Cosmochim. Acta* **65**, 3769 (2001).
34. A. D. Anbar *et al.*, *J. Geophys. Res.* **106**, 3219 (2001).
35. M. A. Zuilen, A. Lepland, G. Arrhenius, *Nature* **418**, 627 (2002).
36. C. F. Chyba, C. Sagan, *Orig. Life* **21**, 3 (1991).
37. G. Ryder, *J. Geophys. Res.* **107**, 5022 (2002).
38. S. G. Love, D. E. Brownlee, *Science* **262**, 550 (1993).
39. P. Ehrenfreund *et al.*, *Rep. Prog. Phys.* **65**, 1427 (2002).


40. We thank two anonymous reviewers and J. F. Kasting for valuable comments. This study was supported by the NASA Astrobiology Institute.


**Supporting Online Material**
www.sciencemag.org/cgi/content/full/1106983/DC1
Materials and Methods
SOM Text
References


1 November 2004; accepted 24 March 2005
Published online 7 April 2005;
10.1126/science.1106983
Include this information when citing this paper.


# Lichen-Like Symbiosis 600 Million Years Ago


**Xunlai Yuan,[1] Shuhai Xiao,[2]* T. N. Taylor[3]**



**The fossil record of fungi and lichens is scarce. Here we report the discovery of lichen-like fossils, involving filamentous hyphae closely associated with coccoidal cyanobacteria or algae, preserved in marine phosphorite of the Doushantuo Formation (between 551 and 635 million years old) at Weng'an, South China. These fossils indicate that fungi developed symbiotic partnerships with photoautotrophs before the evolution of vascular plants.**


Fungi are a major eukaryote kingdom and perform critical ecological roles in nutrient recycling. Many living fungi maintain facultative or obligate interactions with marine and terrestrial photoautotrophs (*1*, *2*). However, the fossil record of fungi is poor and includes Ordovician [460 million years ago (Ma)] glomaleans (*3*) and microfossils interpreted as probable fungi dating to >720 Ma (*4*). Fossil evidence for fungal interactions (such as cyanolichenization, mycoparasitism, and vesicular arbuscular mycorrhizal symbiosis) with other organisms comes from the ~400-million-year-old Rhynie chert in Scotland, which also preserves a diverse


[1]Nanjing Institute of Geology and Palaeontology, Nanjing 210008, China. [2]Department of Geosciences, Virginia Polytechnic Institute and State University, Blacksburg, VA 24061, USA. [3]Department of Ecology and Evolutionary Biology, University of Kansas, Lawrence, KS 66045, USA.

*To whom correspondence should be addressed. E-mail: xiao@vt.edu

fungal assemblage, including chytridiomycetes and ascomycetes (*5*). In addition, some Ediacara fossils (575 to 542 Ma) have been interpreted, on the basis of taphonomic observations, as fungi (*6*) and lichens (*7*).

Here we describe three specimens of lichen-like fossils occurring in thin sections of two phosphorite samples from the upper Doushantuo Formation at Weng'an, South China (*8*) (fig. S1). The samples were collected from a 0.5- to 5-m-thick unit of black bituminous phosphorite immediately above a karstification surface in the middle Doushantuo Formation (*9*). This unit was probably deposited in a shallow subtidal environment and contains abundant algal fossils (*10*, *11*). The Doushantuo Formation in the Yangtze Gorges area is bracketed by U-Pb ages between 635 ± 1 and 551 ± 1 Ma (*12*), and direct Pb-Pb dating of upper Doushantuo phosphorite at Weng'an indicates that the fossils described here are probably 599 ± 4 million years old (*13*); however, Condon and colleagues argue that the fossiliferrous upper Doushantuo Formation may be between 580 and 551 million years old (*8*, *12*).

The lichen-like fossils are completely phosphatized. They consist of two closely associated components: coccoidal cells and thin filaments (Figs. 1 and 2). The coccoid cells are 6 to 15 μm in diameter (average = 9 μm, SD = 2 μm, $n$ = 25 cells) and are usually clustered (Figs. 1A, 2A, and 2C). They typically consist of an opaque central body surrounded by a hyaline envelope 1 to 2 μm thick (Fig. 2E). In some, the remains of organic sheaths are visible in the hyaline envelope. These coccoidal cells are interpreted as sheathed cyanobacteria (similar to modern *Gloeocapsa*, *Entophysalis*, *and Chroococcus*) or possibly green algae (similar to modern colonial chlorococcaleans).

The filaments are about 0.5 to 0.9 μm wide (average = 0.6 μm, SD = 0.1 μm, $n$ = 20 filaments). They are up to 50 μm long, although they may be longer, because the 30-μm-thick thin section captures only a segment of the filaments. It is unclear whether they are septate, because they are opaque. Some filaments branch dichotomously (Fig. 2, E and G). Many bear opaque, pyriform terminal structures (Fig. 2, B and D to F) that are smaller than the coccoidal cells described above, about 3 to 6 μm in maximum dimension (average = 5 μm, SD = 1 μm, $n$ = 6 terminal structures) and 2 to 4 μm in minimum dimension (average = 3 μm, SD = 1 μm, $n$ = 6 terminal structures). Some terminal structures show evidence of possible transverse splits (Fig. 2, D to E). A number of filaments appear to envelop coccoidal cells or are arranged in loops (Fig. 2C). In some cases, a single filament connects two pyriform structures, or a single pyriform structure is connected to multiple filamentous appendages. The filaments lack hyaline sheath-like envelopes that characterize filamentous cyanobacteria, and can be distinguished from pseudoparenchymatous multicellular algae preserved in the same deposit (Fig. 3) (*10*, *11*). In one specimen (Fig. 1A), which was probably fragmented during post-phosphatization reworking, the filaments can be found throughout the entire specimen. In another (Fig. 1B), the filaments occur on only one side of the specimen. However, because the specimens were found in thin sections, it remains impossible to reconstruct the three-dimensional structure of the coccoid/filament association.

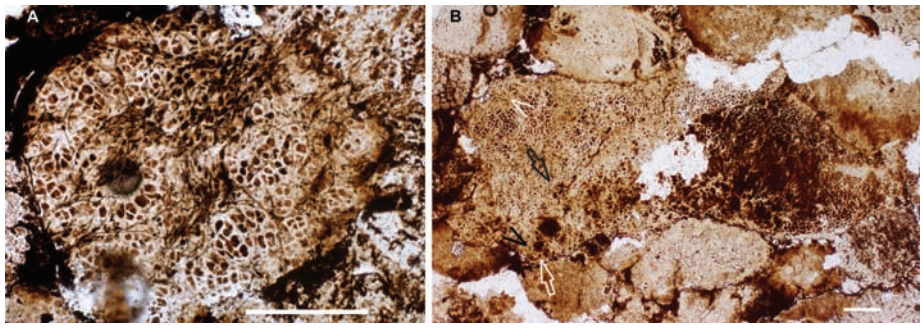


**Fig. 1.** Thin-section photomicrographs of two better-preserved specimens. (**A**) Coccoidal thallus divided by dense filaments in the middle. Further compartmentalization of coccoidal thallus by less densely packed filaments is visible at higher magnification (Fig. 2, A to C). (**B**) Coccoidal thallus with filaments (not discernable at this magnification; see magnified views of arrowed areas in Fig. 2, D to G) in the left part, but not the right part, of this specimen. Scale bars, 100 μm.

We interpret these filaments as fungal hyphae and the pyriform terminal structures as resting spores, reproductive structures, or some type of fungal vesicle. Alternative interpretations (such as filamentous cyanobacteria) are inconsistent with the combination of morphological features (thin filaments, dichotomous branching, pyriform terminal structures, and absence of sheaths). The diameter of the hyphae may have been reduced during phosphatization (*14*), but modern marine fungal hyphae can be <1 μm in diameter (*1*). The pyriform terminal structures are similar to, although smaller than, modern and fossil glomalean spores or vesicles (*2*, *3*, *15*). Furthermore, glomalean (such as *Entrophospora*) hyphae can bear terminal sporiferous saccules and lateral spores (*2*), which are similar to those illustrated in Fig. 2E (white arrowheads).

It is unlikely that the fungal hyphae were saprophytic or were accidentally preserved with the coccoidal cells. In all three specimens, the hyphae are associated only with coccoidal thalli; they do not occur in pseudoparenchymatous red algae in the same deposit (Fig. 3A) (*10*, *11*), which would be expected if they were saprophytic. Furthermore, the coccoidal cells would be expected to show a greater degree of decomposition if the fungal hyphae were saprophytic; instead, the preservation of coccoidal cells is not inferior to that of the fungal hyphae. Third, the hyphae appear to be structurally (and not accidentally) associated with the cyanobacterial coccoids; the coccoid clusters are distinctly compartmentalized and surrounded by abundant hyphae (Figs. 1A, 2A, and 2C) similar to the hyphal nets described in the Devonian cyanolichen (*16*, *17*). This structural association make the coccoidal clusters appear different from structures described as "cell islands" in Doushantuo multicellular algae (*10*); cell islands (Fig. 3B) are surrounded by ellipsoidal cells rather than hyphae. In addition, some hyphae are in close contact with coccoid cells (Fig. 2, C and G), suggesting that there was direct physiological interaction between them.

The association between coccoidal cells and fungal hyphae is interpreted to be symbiotic, not parasitic. The coccoidal thalli show no evidence of host reaction to mycoparasitism. Neither do the coccoid cells in contact with hyphae show morphological abnormality. On the other hand, there are numerous similar coccoidal thalli in the same deposit that are not associated with fungal hyphae (Fig. 3B). Thus, the coccoidal thalli may have functioned as facultative photobionts that could form loose lichen-like or lichenoidal (*1*) association with filamentous mycobionts.

Terrestrial lichens, involving ascomycetes or basidiomycetes as mycobionts and cyanobacteria or chlorophytes as photobionts, have affected global weathering since the Devonian (*5*). Modern marine fungi (mostly ascomycetes) also form a wide range of interactions with cyanobacteria, chlorophytes, phaeophytes, and rhodophytes. These interactions can be loose lichenoidal association with microscopic photobionts, mycophycobiosis with macroscopic algae, mycoparasitism, or obligate lichen association (*1*). Lichenized fungi are phylogenetically widespread within the Dikaryomycota (Ascomycota + Basidiomycota), which suggests that fungal lichenization may have evolved multiple times (*18*–*20*). However, the broadly defined symbiotic life-style (including arbuscular mycorrhizal symbiosis) has a broader phylogenetic distribution and characterizes the Symbiomycota (Glomeromycota + Dikaryomycota) (*21*, *22*). Although most glomerocycetes are arbuscular mycorrhizal fungi with vascular plants,

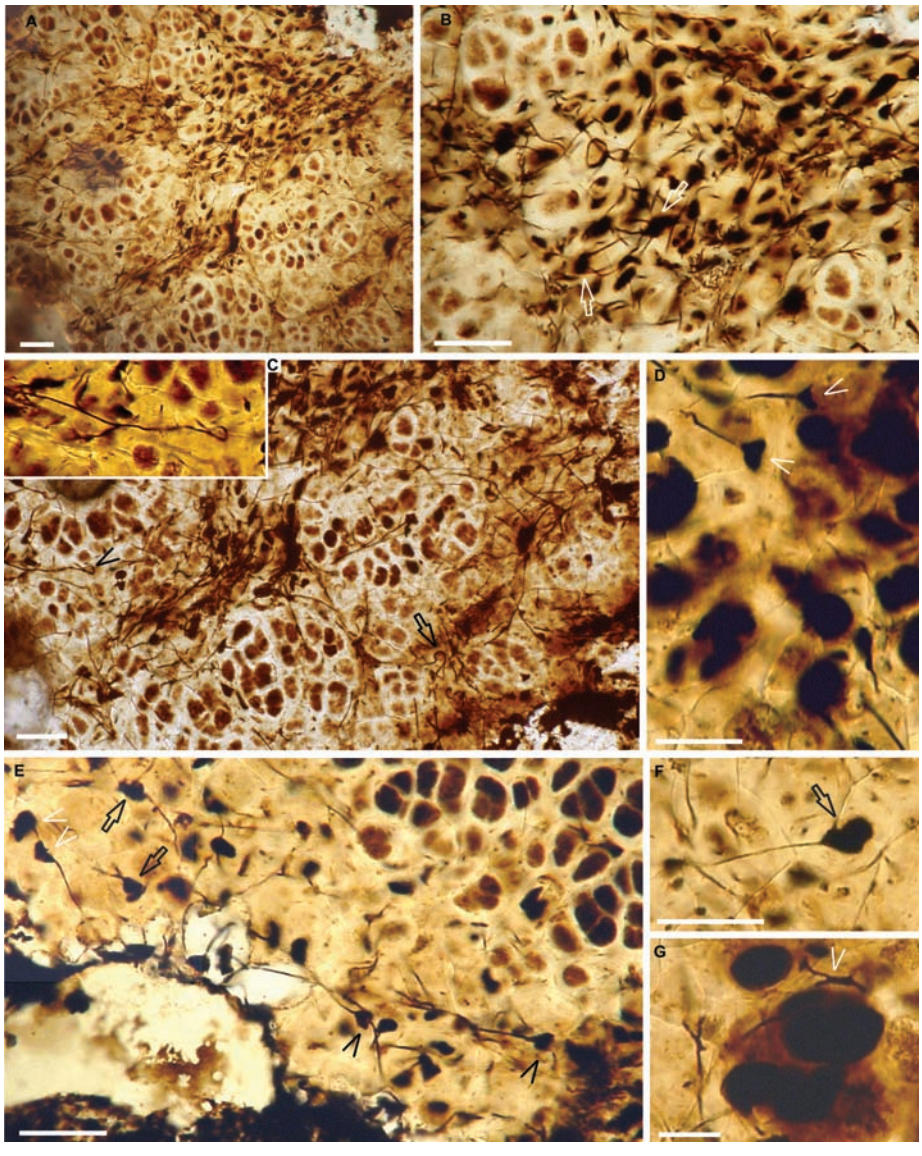


**Fig. 2.** (**A**) Detail of the upper center part of Fig. 1A. (**B**) Detail of the upper right quarter of (A), showing filament tract. Several filaments have dark swollen terminal structures. Arrows indicate terminal structures with multiple filamentous appendages. (**C**) Detail of the center part of (A). Two packets of coccoidal cells (center and lower center) are surrounded by a few filaments. The arrow points to a filament that appears to envelop a coccoidal cell. The arrowhead indicates a filament with a terminal loop (close-up in inset). (**D**) Detail (white arrow in Fig. 1B) showing hyphae with funnel-shaped terminal structures (arrowheads), the distal parts of which were probably dehisced along a transverse split. (**E**) Detail (white arrowhead in Fig. 1B) showing funnel-shaped terminal structures (black arrowheads), clustered coccoidal cells with hyaline envelopes (upper right quarter), dark terminal structures connected to multiple or branching filaments (black arrows), and a filament with a terminal structure and a laterally borne intercalary vesicle (white arrowheads). (**F**) Detail (black arrow in Fig. 1B) showing terminal structure (arrow) with subtending filament. (**G**) Detail (black arrowhead in Fig. 1B) showing branching filament (arrow) in close association with coccoidal cells. Scale bars, 20 μm.

*Geosiphon pyriforme* (a basal glomeromycete) is symbiotic with cyanobacteria (*23*). The ease with which symbionts can be gained, lost, and switched in fungal/photoautotroph associations (*24*, *25*), the fungal phylogenetic tree that is basally populated by aquatic chytrids (*22*), and probably fungal fossils from Proterozoic marine deposits (*4*) indicate that the early steps toward fungal/photoautotroph symbiosis may have begun as facultative interactions with aquatic cyanobacteria or algae. The Doushantuo lichenoidal fossils suggest that these early steps may have occurred long before the colonization of land by vascular plants, in a shallow marine ecosystem where a large number of free-living cyanobacteria, algae, and fungi were in close association—a necessary step in the evolution of symbiosis. Thus, this and other fossil evidence (*4*) join molecular data (*26*, *27*) to support a deep history of fungi and lichen-like symbiosis.

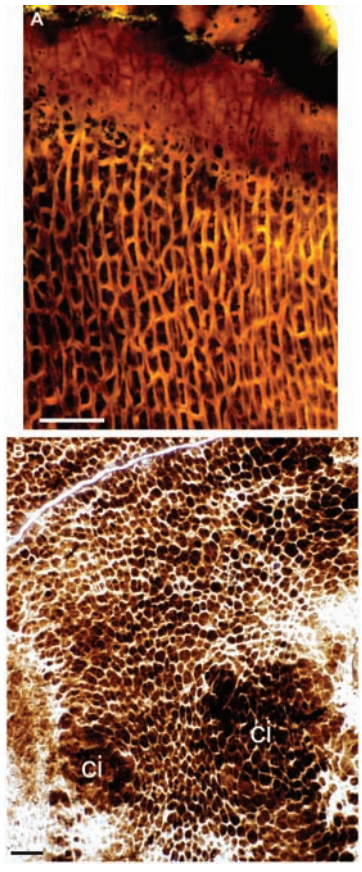


**Fig. 3.** Doushantuo algal thalli with no filamentous symbionts. (**A**) Pseudoparenchymatous red alga (*Thallophyca corrugata*) from the same horizon (*9*, *11*). (**B**) Thallus from the same thin section where lichen-like fossils were found. Emerging cell islands (ci) are indicated. Scale bars, 20 μm.

### References and Notes

1. J. Kohlmeyer, E. Kohlmeyer, *Marine Mycology: The Higher Fungi* (Academic Press, New York, 1979).
2. C. J. Alexopoulos, C. W. Mims, M. Blackwell, *Introductory Mycology* (Wiley, New York, ed. 4, 1996).
3. D. Redecker, R. Kodner, L. E. Graham, *Science* **289**, 1920 (2000).
4. N. J. Butterfield, *Paleobiology* **31**, 165 (2005).
5. T. N. Taylor *et al.*, *Trans. R. Soc. Edinb. Earth Sci.* **94**, 457 (2004).
6. K. J. Peterson, B. Waggoner, J. W. Hagadorn, *Integr. Comp. Biol.* **43**, 127 (2003).
7. G. J. Retallack, *Paleobiology* **20**, 523 (1994).
8. Stratigraphic information is available as supporting material on *Science Online*.
9. Y. Zhang, L. Yin, S. Xiao, A. H. Knoll, *Paleontol. Soc. Mem.* **50**, 1 (1998).
10. Y. Zhang, *Lethaia* **22**, 113 (1989).
11. S. Xiao, A. H. Knoll, X. Yuan, C. M. Pueschel, *Am. J. Bot.* **91**, 214 (2004).
12. D. Condon *et al.*, *Science* **308**, 95 (2005); published online 24 February 2005 (10.1126/science.1107765).
13. G. H. Barfod *et al.*, *Earth Planet. Sci. Lett.* **201**, 203 (2002).
14. A. H. Knoll, S. Golubic, *Precambrian Res.* **10**, 115 (1979).
15. T. N. Taylor, W. Remy, H. Hass, H. Kerp, *Mycologia* **87**, 560 (1995).
16. T. N. Taylor, H. Hass, W. Remy, H. Kerp, *Nature* **378**, 244 (1995).
17. T. N. Taylor, H. Hass, H. Kerp, *Am. J. Bot.* **84**, 992 (1997).

18. A. Gargas, P. T. Depriest, M. Grube, A. Tehler, *Science* **268**, 1492 (1995).
19. F. Lutzoni, M. Pagel, V. Reeb, *Nature* **411**, 937 (2001).
20. Y. J. Liu, B. D. Hall, *Proc. Natl. Acad. Sci. U.S.A.* **101**, 4507 (2004).
21. A. Schüßler, D. Schwarzott, C. Walker, *Mycol. Res.* **105**, 1413 (2001).
22. A. Tehler, D. P. Little, J. S. Farris, *Mycol. Res.* **107**, 901 (2003).
23. H. Gehrig, A. Schüßler, M. Kluge, *J. Mol. Evol.* **43**, 71 (1996).
24. P. T. DePriest, *Annu. Rev. Microbiol.* **58**, 273 (2004).
25. M. Wedin, H. Döring, G. Gilenstam, *New Phytol.* **164**, 459 (2004).
26. M. L. Berbee, J. W. Taylor, in *The Mycota: A Comprehensive Treatise on Fungi as Experimental Systems for Basic and Applied Research*, D. J. McLaughlin, E. G. McLaughlin, P. A. Lemke, Eds. (Springer-Verlag, Berlin, 2001), pp. 229–245.
27. D. S. Heckman *et al.*, *Science* **293**, 1129 (2001).


28. This research was supported by the National Natural Science Foundation of China, U.S. NSF, Chinese Academy of Sciences, and Chinese Ministry of Science and Technology. We thank M. Kowalewski, S. E. Scheckler, C. M. Zhou, and four anonymous reviewers for valuable comments.


**Supporting Online Material**
www.sciencemag.org/cgi/content/full/308/5724/1017/DC1
SOM Text
Fig. S1
References


22 February 2005; accepted 29 March 2005
10.1126/science.1111347


# The Structure of a pH-Sensing Mycobacterial Adenylyl Cyclase Holoenzyme


**Ivo Tews,[1]*† Felix Findeisen,[1]* Irmgard Sinning,[1] Anita Schultz,[2] Joachim E. Schultz,[2] Jürgen U. Linder[2]†**



**Class III adenylyl cyclases contain catalytic and regulatory domains, yet structural insight into their interactions is missing. We show that the mycobacterial adenylyl cyclase Rv1264 is rendered a pH sensor by its N-terminal domain. In the structure of the inhibited state, catalytic and regulatory domains share a large interface involving catalytic residues. In the structure of the active state, the two catalytic domains rotate by 55° to form two catalytic sites at their interface. Two α helices serve as molecular switches. Mutagenesis is consistent with a regulatory role of the structural transition, and we suggest that the transition is regulated by pH.**


Adenylyl cyclases (ACs) synthesize the universal second messenger 3′,5′-cyclic adenosine monophosphate (cAMP) (*1*). Most ACs belong to class III, such as all mammalian and many bacterial enzymes (*2*), and are multidomain proteins (*2*, *3*). In the genome of the bacterium *Mycobacterium tuberculosis* (*4*), 15 putative class III ACs (*5*) with eight different domain compositions have been identified. For comparison, the similarly sized genome of *Escherichia coli* contains a single AC gene, and even in the human genome only 10 AC genes have been identified (*6*, *7*). This suggests that mycobacteria can respond to changing extra- and intracellular conditions by cAMP formation.

The mycobacterial AC Rv1264 is autoinhibited by its N-terminal domain (*8*). A knockout of the single *Streptomyces* AC, which has an identical domain composition to Rv1264, abolishes the bacterial response to an acidic milieu that affects differentiation processes (*9*). Because *M. tuberculosis* must counteract acidification of phagolysosomes during host invasion for intracellular survival (*10*, *11*), we examined the pH sensitivity of Rv1264 (Fig. 1A) (*12*). At pH 8, AC activity was 3 nmol of cAMP•mg$^{-1}$•min$^{-1}$ at 0.5 mM adenosine triphosphate (ATP) with a maximal velocity ($V_{max}$) of 34 nmol of cAMP•mg$^{-1}$•min$^{-1}$ and a substrate affinity ($SC_{50}$) of 1.5 mM ATP. At pH 6, AC activity increased almost 40-fold to 115 nmol and $V_{max}$ increased 12-fold to 420 nmol of cAMP•mg$^{-1}$•min$^{-1}$. The substrate affinity increased slightly to 0.8 mM ATP. The Hill coefficient of 1.9 was unaffected. In contrast, the isolated catalytic domain ($Rv1264_{211-397}$) displayed uniformly high AC activity between pH 5.5 and 8 (Fig. 1A). Thus, in Rv1264, pH sensitivity is mediated by a distinct regulatory domain, and the activation by far exceeds the usual pH dependence of an enzyme. Biochemically, Rv1264 qualifies as a pH-sensing AC and is a likely candidate for mycobacterial pH sensing.

To understand the molecular mechanism of pH sensing and AC regulation, two crystal forms of Rv1264 were analyzed (*12*). Anisotropic crystals in a hexagonal space group with a diffraction limit of 3.3 Å were grown from $Li_2SO_4$, and the resulting model was designated the active form of Rv1264 (Fig. 2A); the 2.3 Å resolution structure obtained from monoclinic crystals grown from polyethylene glycol was designated the inhibited

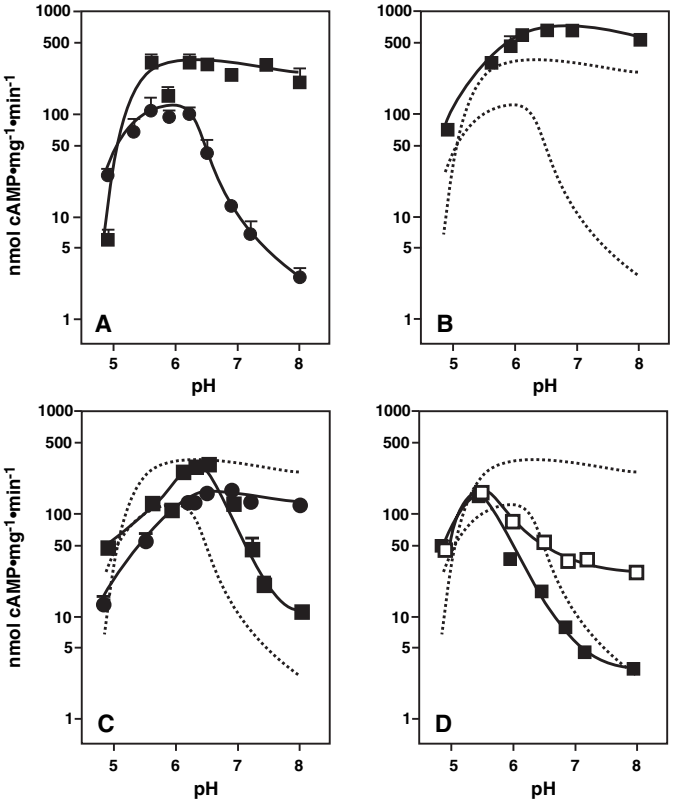


**Fig. 1.** The pH dependence of the AC activity of the Rv1264 wild type and mutants. AC activities of purified recombinant enzymes were measured from pH 4.8 to 8.0, with 0.5 mM ATP as a substrate. Standard deviation (SD) is given by error bars, if they exceed the size of the symbols. The symbol size itself corresponds to an SD of 10%. (**A**) Rv1264 catalytic domain ($Rv1264_{211-397}$) (■) and holoenzyme (●). To facilitate comparisons, these curves are included as dotted lines in the other panels. (**B**) Rv1264 M193P/M194P (■). (**C**) Rv1264 R309A (●) and E195A (■). (**D**) Rv1264 H192A (■) and H192E (□).


[1]Biochemiezentrum der Universität Heidelberg, Im Neuenheimer Feld 328, 69120 Heidelberg, Germany. [2]Pharmazeutisches Institut, Pharmazeutische Biochemie, Morgenstelle 8, 72076 Tübingen, Germany.

*These authors contributed equally to this work.
†To whom correspondence should be addressed. E-mail: ivo.tews@bzh.uni-heidelberg.de (I.T.); juergen.linder@uni-tuebingen.de (J.U.L.)